

Well-balanced semi-implicit scheme for the Euler equations with gravity

BOUHENNICHE Oussama

Supervisors:

Ms. Andrea THOMANN

Mr. Victor MICHEL-DANSAC

August 22, 2025

Inria, University of Strasbourg, France

Table of contents

Introduction

The Euler equations with gravity

The numerical scheme

Implementation

Numerical Results

Well-balanced tests

Accuracy

Conclusion

Bibliography

Host Organization

- This internship is a final-year project for the Master 2 program in Scientific Computing and Mathematical Innovation.
- It is a five-month internship, carried out within the Macaron team (MACHINE leARNING for Optimized Numerical methods) at Inria Nancy–Grand Est, hosted in Strasbourg.
- The internship was funded by ITI IRMIA++.



Introduction

Context & Problematic

- Many natural phenomena (geophysical and astrophysical flows) are modeled by the compressible Euler equations with gravitational source terms.
- Gravity generates hydrostatic equilibria where the pressure gradient balances the gravitational force.
- A major difficulty: many flows evolve in the **low-Mach regime**, where $|\mathbf{u}| \ll c$ (flow velocity much smaller than speed of sound).
- Explicit schemes face two main challenges:
 - (i) Acoustic CFL restriction \Rightarrow prohibitively small time steps.
 - (ii) Lack of preservation of hydrostatic equilibria \Rightarrow spurious oscillations and instabilities.

Objectives

The objective of this internship is the development of a **well-balanced semi-implicit scheme** for the compressible Euler equations with gravity.

The method relies on:

- Flux-splitting: explicit discretization of transport terms, implicit treatment of pressure and gravity.
- Implicit step formulated as a linear elliptic problem (pressure or total energy).
- IMEX Runge–Kutta methods for high-order accuracy in time.
- Finite volume discretization on Cartesian grids.

Our proposed scheme is designed to:

1. Remove the acoustic time step restriction.
2. Preserve hydrostatic equilibria exactly.
3. Remain asymptotic-preserving in the low-Mach regime.

The Euler equations with gravity

Classical Euler Equations

- Euler equations [2] are a cornerstone of fluid dynamics.
- They describe compressible, inviscid fluid motion based on:
 - Conservation of mass
 - Conservation of momentum
 - Conservation of energy

Classical form:

$$\partial_t \rho + \nabla \cdot (\rho \mathbf{u}) = 0,$$

$$\partial_t (\rho \mathbf{u}) + \nabla \cdot (\rho \mathbf{u} \otimes \mathbf{u}) + \nabla p = 0,$$

$$\partial_t (\rho E) + \nabla \cdot (\mathbf{u}(\rho E + p)) = 0.$$

Where the total energy density is given by:

$$\rho E = \rho e + \frac{1}{2} \rho \|\mathbf{u}\|^2$$

Euler Equations with Gravity

- In presence of a gravitational potential ϕ , momentum equation include source terms.
- Using suitable reference scales, we nondimensionalize the equations, introducing the Mach and Froude numbers:
- The non-dimensional system reads:

$$\partial_t \rho + \nabla \cdot (\rho \mathbf{u}) = 0,$$

$$\partial_t (\rho \mathbf{u}) + \nabla \cdot (\rho \mathbf{u} \otimes \mathbf{u}) + \frac{1}{M^2} \nabla p = -\frac{1}{Fr^2} \rho \nabla \phi,$$

$$\partial_t E + \nabla \cdot (\mathbf{u}(E + p)) = 0,$$

with the total energy

$$E = \rho e + \frac{1}{2} M^2 \rho \|\mathbf{u}\|^2 + \frac{M^2}{Fr^2} \rho \phi.$$

Hydrostatic Equilibria and Low-Mach Limit

- **Hydrostatic equilibrium:**

$$\mathbf{u} = 0, \quad \frac{1}{M^2} \nabla p = -\frac{1}{Fr^2} \rho \nabla \phi$$

- Examples:
 - Isothermal atmosphere: exponential profiles
 - Polytropic atmosphere: power-law profiles
- **Low-Mach limit:** $M \rightarrow 0$ with $M \sim Fr \Rightarrow$ Dynamics evolve on slow time scales governed by transport and buoyancy.
- Numerical difficulty:
 - Acoustic CFL \Rightarrow very small time steps
 - Numerical viscosity overdamps slow modes

The numerical scheme

Semi-implicit well-balanced scheme: overview

- Goal: develop a **semi-implicit well-balanced** scheme for Euler with gravity.
- Key ideas:
 - Explicit treatment for **transport/convective** terms.
 - Implicit treatment for **stiff pressure** and **gravity** to remove acoustic CFL.
 - Exact preservation of hydrostatic equilibria (**well-balanced**).
- Roadmap:
 1. Well-balanced reformulation
 2. Time semi-discrete scheme
 3. Fully discrete finite-volume scheme
 4. High-order (IMEX-RK) extension

Well-balanced reformulation

Assume a known hydrostatic equilibrium (ρ^{hyd}, p^{hyd}) :

$$\frac{\nabla p^{hyd}}{M^2} = -\rho^{hyd} \frac{\nabla \phi}{Fr^2}.$$

It implies

$$\nabla \phi = -\frac{Fr^2}{M^2} \frac{\nabla p^{hyd}}{\rho^{hyd}}.$$

Plugging into the Euler system yields

$$\partial_t \rho + \nabla \cdot (\rho \mathbf{u}) = 0,$$

$$\partial_t(\rho \mathbf{u}) + \nabla \cdot (\rho \mathbf{u} \otimes \mathbf{u}) + \frac{1}{M^2} \nabla p = \frac{\rho}{\rho^{hyd}} \frac{1}{M^2} \nabla p^{hyd},$$

$$\partial_t E + \nabla \cdot (\mathbf{u}(E + p)) = 0.$$

Flux splitting: explicit vs. implicit

Conservative variables vector:

$$\mathbf{q} = \begin{pmatrix} \rho \\ \rho \mathbf{u} \\ E \end{pmatrix}.$$

We split flux/source as:

$$\mathbf{f}(\mathbf{q}) = \underbrace{\mathbf{f}^u(\mathbf{q})}_{\text{explicit}} + \underbrace{\mathbf{f}^p(\mathbf{q})}_{\text{implicit}}, \quad \mathbf{s}(\mathbf{q}) = \underbrace{\mathbf{s}^p(\mathbf{q})}_{\text{implicit}}.$$

$$\mathbf{f}^u(\mathbf{q}) = \begin{pmatrix} \rho \mathbf{u} \\ \rho \mathbf{u} \otimes \mathbf{u} \\ 0 \end{pmatrix}, \quad \mathbf{f}^p(\mathbf{q}) = \begin{pmatrix} 0 \\ \frac{p}{M^2} \mathbb{I} \\ \mathbf{u}(E + p) \end{pmatrix}, \quad \mathbf{s}^p(\mathbf{q}) = \begin{pmatrix} 0 \\ \frac{\rho}{\rho^{hyd}} \frac{1}{M^2} \nabla p^{hyd} \\ 0 \end{pmatrix}.$$

Gravity grouped with the implicit part \Rightarrow well-balanced at discrete level.

Time semi-discrete semi-implicit scheme

Semi-discrete form:

$$\partial_t \mathbf{q} + \nabla \cdot \mathbf{f}^u(\mathbf{q}) + \nabla \cdot \mathbf{f}^p(\mathbf{q}) = \mathbf{s}^p(\mathbf{q}).$$

First-order (in time) scheme:

$$\rho^{n+1} - \rho^n + \Delta t \nabla \cdot (\rho \mathbf{u})^n = 0,$$

$$(\rho \mathbf{u})^{n+1} - (\rho \mathbf{u})^n + \Delta t \nabla \cdot (\rho \mathbf{u} \otimes \mathbf{u})^n + \frac{\Delta t}{M^2} \nabla p^{n+1} = \frac{\rho^{n+1}}{\rho^{hyd}} \frac{\Delta t}{M^2} \nabla p^{hyd},$$

$$E^{n+1} - E^n + \Delta t \nabla \cdot ((\rho \mathbf{u})^{n+1} H^n) = 0,$$

with enthalpy $H^n = \frac{E^n + p^n}{\rho^n}$.

Time step: explicit & implicit update

Stage 1: explicit

$$\begin{aligned}\rho^{(1)} &= \rho^n - \Delta t \nabla \cdot (\rho \mathbf{u})^n, \\ (\rho \mathbf{u})^{(1)} &= (\rho \mathbf{u})^n - \Delta t \nabla \cdot (\rho \mathbf{u} \otimes \mathbf{u})^n, \\ E^{(1)} &= E^n.\end{aligned}$$

Density is fully explicit: $\rho^{n+1} = \rho^{(1)}$.

Stage 2: implicit

$$\begin{aligned}(\rho \mathbf{u})^{n+1} &= (\rho \mathbf{u})^{(1)} - \frac{\Delta t}{M^2} \nabla p^{n+1} + \frac{\rho^{n+1}}{\rho^{hyd}} \frac{\Delta t}{M^2} \nabla p^{hyd}, \\ E^{n+1} &= E^{(1)} - \Delta t \nabla \cdot ((\rho \mathbf{u})^{n+1} H^n).\end{aligned}$$

Plugging momentum equation in energy equations yields a *linear elliptic* problem

$$E^{n+1} = E^{(1)} - \Delta t \nabla \cdot (H^n (\rho \mathbf{u})^{(1)}) + \frac{\Delta t^2}{M^2} \nabla \cdot (H^n \nabla p^{n+1}) - \frac{\Delta t^2}{M^2} \nabla \cdot \left(H^n \frac{\rho^{n+1}}{\rho^{hyd}} \nabla p^{hyd} \right),$$

then use a linearized EOS to obtain an **energy-based** or **pressure-based** approach.

Two closures: energy-based vs. pressure-based

- **Energy-based:** solve the elliptic problem for E^{n+1} , recover p^{n+1} via the linearized EOS.
- **Pressure-based:** recast the elliptic equation in terms of p^{n+1} via the EOS, solve for p^{n+1} , then update $(\rho \mathbf{u})^{n+1}$ and reconstruct E^{n+1} .

Following [1] We choose this linearizations of EOS for each approach:

$$\text{Energy-based: } p^{n+1} = (\gamma - 1) \left(E^{n+1} - M^2 (\rho E_{\text{kin}})^n - \frac{M^2}{Fr^2} (\rho E_{\text{pot}})^{n+1} \right).$$

$$\text{Pressure-based: } p^{n+1} = (\gamma - 1) \left(E^{n+1} - M^2 (\rho E_{\text{kin}})^n - \frac{M^2}{Fr^2} (\rho E_{\text{pot}})^n \right).$$

Energy-based closure

Substitute EOS into the elliptic step:

$$E^{n+1} - (\gamma - 1) \frac{\Delta t^2}{M^2} \nabla \cdot (H^n \nabla E^{n+1}) = E^{(1, \star)},$$

with

$$\begin{aligned} E^{(1, \star)} = E^{(1)} - \Delta t \nabla \cdot (H^n (\rho \mathbf{u})^{(1)}) - \frac{\Delta t^2}{M^2} \nabla \cdot \left(H^n \frac{\rho^{n+1}}{\rho^{hyd}} \nabla p^{hyd} \right) \\ - (\gamma - 1) \frac{\Delta t^2}{M^2} \nabla \cdot \left(H^n \nabla \left(M^2 (\rho E_{kin})^n + \frac{M^2}{Fr^2} (\rho E_{pot})^{n+1} \right) \right). \end{aligned}$$

Then update momentum with p^{n+1} from EOS, then (for consistency) recompute E^{n+1} using the fully implicit flux.

Pressure-based closure

Express energy via pressure:

$$E^{n+1} = \frac{p^{n+1}}{\gamma - 1} + M^2(\rho E_{\text{kin}})^n + \frac{M^2}{Fr^2}(\rho E_{\text{pot}})^n.$$

Elliptic problem for p^{n+1} :

$$p^{n+1} - (\gamma - 1) \frac{\Delta t^2}{M^2} \nabla \cdot (H^n \nabla p^{n+1}) = p^{(1, \star)},$$

$$p^{(1, \star)} = p^{(1)} - (\gamma - 1) \Delta t \nabla \cdot (H^n (\rho \mathbf{u})^{(1)}) - (\gamma - 1) \frac{\Delta t^2}{M^2} \nabla \cdot \left(H^n \frac{\rho^{n+1}}{\rho^{hyd}} \nabla p^{hyd} \right).$$

Then update $(\rho \mathbf{u})^{n+1}$ and E^{n+1} .

Fully discrete finite-volume scheme

- **Framework:** fully discrete **finite-volume** method on a Cartesian grid (cell averages).
- **Explicit transport: Rusanov (LLF)** numerical flux.
- **Implicit pressure-gravity:**
 - divergence: **centered** numerical flux (zero artificial viscosity),
 - gradient: **centered differences** (2nd order).
- **Div-grad operator:** centered discrete operator $\mathcal{H}[h, q] \approx \nabla \cdot (h \nabla q)$ (2nd order).
- **CFL:** time step constrained *only* by the explicit transport subsystem.

Second-order IMEX-RK (ARS(3,3,2))

ARS(3,3,2) Butcher tables (with $\beta = 1 - \frac{\sqrt{2}}{2}$):

explicit	0	0	0	0
	β	β	0	0
	1	$\beta - 1$	$2 - \beta$	0
		$\beta - 1$	$2 - \beta$	0

implicit	0	0	0	0
	β	0	β	0
	1	0	$1 - \beta$	β
		0	$1 - \beta$	β

IMEX-RK stages:

$$\mathbf{q}^{(k)} = \mathbf{q}^n - \Delta t \sum_{l=1}^{k-1} \tilde{a}_{kl} \nabla \cdot f^e(\mathbf{q}^{(l)}) - \Delta t \sum_{l=1}^k a_{kl} (\nabla \cdot f^i(\mathbf{q}^{(l)}) + \mathbf{s}(\mathbf{q}^{(l)})).$$

Update:

$$\mathbf{q}^{n+1} = \mathbf{q}^n - \Delta t \sum_{k=1}^s \tilde{b}_k \nabla \cdot f^e(\mathbf{q}^{(k)}) - \Delta t \sum_{k=1}^s b_k (\nabla \cdot f^i(\mathbf{q}^{(k)}) + \mathbf{s}(\mathbf{q}^{(k)})).$$

We use **MUSCL** linear reconstruction to achieve **second-order** accuracy in space.

Implementation

Implementation: Overview

- The numerical scheme is implemented in a **modular, reproducible** way and managed in a private GitLab repository.
- The solver is a **Python package** with dedicated modules for:
 - **Mesh handling**
 - **Discretization** (FV operators, reconstructions)
 - **Numerical fluxes**
 - **Time integration** (semi-implicit / IMEX-RK)
 - **Post-processing** (I/O, visualization)
- A suite of **benchmark test cases** are implemented; all are **fully parameterizable** (domain, BCs, numerical parameters).

Implementation: Implicit Solver & HPC

- **Implicit step (elliptic pressure equation):** the discrete operator matrix is **assembled explicitly**, enabling robust preconditioning.
- Use of **BiCGStab** Krylov solver with **ILU** preconditioner to improves stability and accelerates convergence in the **low-Mach** regime (stiff elliptic systems).
- **Execution environment:** simulations run on the **Gaya** HPC cluster

Numerical Results

Numerical results overview

- **Well-balanced tests:** Isothermal and polytropic hydrostatic atmospheres.
- **Accuracy:** Graf–Gresho vortex with gravity.
- **Vanishing-gravity / Euler limit:** Sod shock tube; Kelvin–Helmholtz instability.
- **Instability benchmarks:** Rayleigh–Taylor, rising thermal bubble, shock–bubble interaction.

Well-balanced tests: setup

- 2D stationary atmospheres (isothermal & polytropic), advanced with the **second-order** scheme.
- Uniform grid 100×100 on $[0, 1] \times [0, 1]$, final time $T_f = 1.0$, exact boundary conditions.
- Potential $\phi(x, y) = \frac{1}{2}(x + y)$, adiabatic index $\gamma = 1.4$.
- Errors measured in L^1 against the corresponding hydrostatic state.

Isothermal atmosphere

$$\text{Hydrostatic state: } \rho^{\text{hyd}}(x, y) = \exp\left(-\frac{M^2}{Fr^2} \phi(x, y)\right), \quad p^{\text{hyd}}(x, y) = \rho^{\text{hyd}}(x, y).$$

	Energy-based			Pressure-based		
	ρ	$\ \mathbf{u}\ $	E	ρ	$\ \mathbf{u}\ $	E
$M = 1$	4.71e-13	7.83e-14	7.25e-12	4.71e-13	9.36e-14	8.09e-12
$M = 10^{-5}$	5.99e-13	1.01e-13	9.70e-12	6.51e-13	6.30e-14	5.66e-12
$M = 10^{-10}$	6.84e-13	9.99e-14	9.92e-12	4.32e-13	7.00e-14	6.72e-12

Table 1: L^1 errors for the isothermal atmosphere with $Fr = M$.

The cases $Fr = 0.75 M$ and $Fr = 10 M$ exhibit the same round-off-level behavior.

Polytropic atmosphere

Hydrostatic state:

$$\rho^{\text{hyd}}(x, y) = \left(1 - \frac{\gamma-1}{\gamma} \frac{M^2}{Fr^2} \phi(x, y)\right)^{\frac{1}{\gamma-1}}, \quad p^{\text{hyd}}(x, y) = \left(1 - \frac{\gamma-1}{\gamma} \frac{M^2}{Fr^2} \phi(x, y)\right)^{\frac{\gamma}{\gamma-1}}.$$

	Energy-based ($Fr = M$)			Pressure-based ($Fr = M$)		
	ρ	$\ \mathbf{u}\ $	E	ρ	$\ \mathbf{u}\ $	E
$M = 1$	1.17e-12	2.10e-13	1.69e-11	7.17e-13	6.35e-14	4.91e-12
$M = 10^{-5}$	7.48e-13	1.38e-13	1.20e-11	7.33e-13	1.39e-13	1.09e-11
$M = 10^{-10}$	1.08e-12	1.78e-13	1.57e-11	7.55e-13	6.90e-14	5.46e-12

Table 2: L^1 errors for the polytropic atmosphere with $Fr = M$.

Remark. The cases $Fr = 0.75 M$ and $Fr = 10 M$ display the same (round-off-level) behavior.

Graf–Gresho vortex — setup

Configuration. Domain $[0, 1] \times [0, 1]$, periodic BCs, $\gamma = 1.4$, grid 128×128 , final time $T_f = 1$ (one turn), parameters $M = Fr = 10^{-2}$.

Pressure split (background + perturbation):

$$p(r) = p_0(r) + M^2 p_2(r), \quad p_0 = RT \rho, \quad \rho(r) = \exp\left(-\frac{M^2}{Fr^2 RT} \phi(r)\right).$$

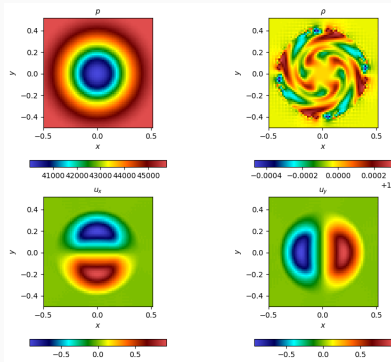
p_0 : hydrostatic background in balance with gravity. p_2 : vortex-induced pressure correction.

Angular velocity profile:

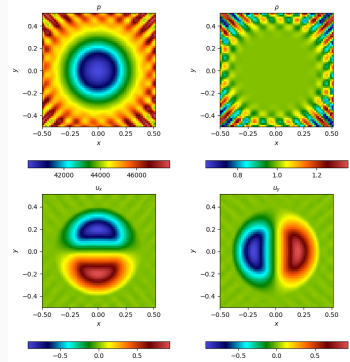
$$u_\theta(r) = \frac{1}{u_r} \begin{cases} 5r, & r \leq 0.2, \\ 2 - 5r, & 0.2 < r \leq 0.4, \\ 0, & r > 0.4. \end{cases}$$

Velocity field: $\mathbf{u}(x, y) = u_\theta(r)(-\sin \theta, \cos \theta)^\top$, $\theta = \arctan 2(y, x)$.

Graf-Gresho vortex results at $t = 1$



(a) Energy-based scheme.



(b) Pressure-based scheme

Figure 2: Graf-Gresho vortex results at $t = 1$

Accuracy benchmark: Graf–Gresho vortex

Why this case?

- Taken from [7]. Probes **well-balancedness**, **low-Mach robustness**, **AP behavior**, and **EOC**.

Setup (non-dimensional).

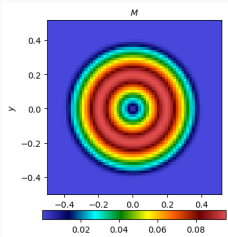
- Periodic domain $[0, 1]^2$; final time $T_f = 1$ (one revolution); $\gamma = 1.4$.
- Mach/Froude: $M = Fr \in \{10^{-1}, 10^{-2}, 10^{-3}, 10^{-4}\}$.

Metrics.

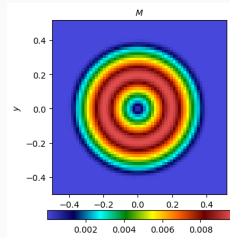
- L^1 errors in ρ , $\rho \mathbf{u}$, E and experimental order of convergence (EOC).
- Loss of kinetic energy after one turn (dissipation indicator).
- Stability as M decreases (evidence of AP behavior).

$M = Fr$	N	ρ		ρU_x		ρU_y		ρE	
10^{-1}	25	8.230E-04	–	1.058E-02	–	1.058E-02	–	1.379E-03	–
	50	1.648E-04	2.32	2.681E-03	1.98	2.681E-03	1.98	2.016E-04	2.77
	100	4.111E-05	2.00	1.000E-03	1.42	1.000E-03	1.42	5.650E-05	1.83
	200	1.130E-05	1.86	3.593E-04	1.48	3.593E-04	1.48	2.240E-05	1.34
10^{-2}	25	6.559E-04	–	1.025E-02	–	1.025E-02	–	1.229E-03	–
	50	1.168E-04	2.49	2.622E-03	1.97	2.622E-03	1.97	1.320E-04	3.22
	100	3.101E-05	1.91	9.884E-04	1.41	9.884E-04	1.41	2.809E-05	2.23
	200	8.746E-06	1.83	3.565E-04	1.47	3.565E-04	1.47	8.093E-06	1.80
10^{-3}	25	6.424E-04	–	1.022E-02	–	1.022E-02	–	1.261E-03	–
	50	9.818E-05	2.71	2.622E-03	1.96	2.622E-03	1.96	1.188E-04	3.41
	100	2.528E-05	1.96	9.879E-04	1.41	9.879E-04	1.41	2.495E-05	2.25
	200	7.423E-06	1.77	3.565E-04	1.47	3.565E-04	1.47	7.532E-06	1.73
10^{-4}	25	6.427E-04	–	1.022E-02	–	1.022E-02	–	1.262E-03	–
	50	9.876E-05	2.70	2.622E-03	1.96	2.622E-03	1.96	1.189E-04	3.41
	100	2.545E-05	1.96	9.880E-04	1.41	9.880E-04	1.41	2.497E-05	2.25
	200	7.387E-06	1.78	3.565E-04	1.47	3.565E-04	1.47	7.514E-06	1.73

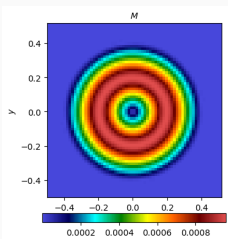
Table 3: L^1 errors and convergence rates for various values of M and Fr using the Energy-based scheme.



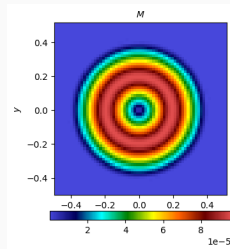
(a) $M = 10^{-1}$



(b) $M = 10^{-2}$



(c) $M = 10^{-3}$



(d) $M = 10^{-4}$

Figure 3: Mach number distribution for different maximal Mach numbers for energy-based schema

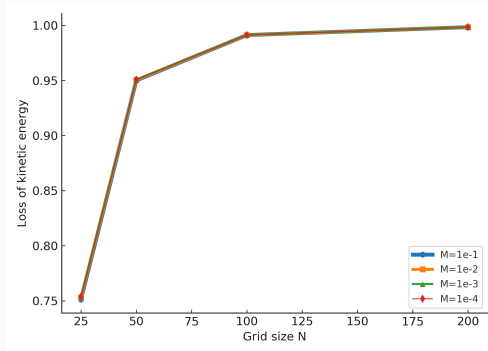


Figure 4: Loss of kinetic energy for different grids and Mach numbers

Sod shock tube problem

Setup.

- 1D Euler (no gravity) on $[0, 1]$, discontinuity at $x = 0.5$.
- Initial states (ρ, u, p) :

$$(1, 0, 1) \text{ for } x < 0.5, \quad (0.125, 0, 0.1) \text{ for } x > 0.5.$$

- $\gamma = 1.4$, $M = 1$, final time $t = 0.1644$, grid $N_x = 75$.
- Reference (“exact”) solution from open-source Riemann solver .

Expected pattern. Left rarefaction, mid contact, right shock [6].

Sod shock tube: numerical vs exact

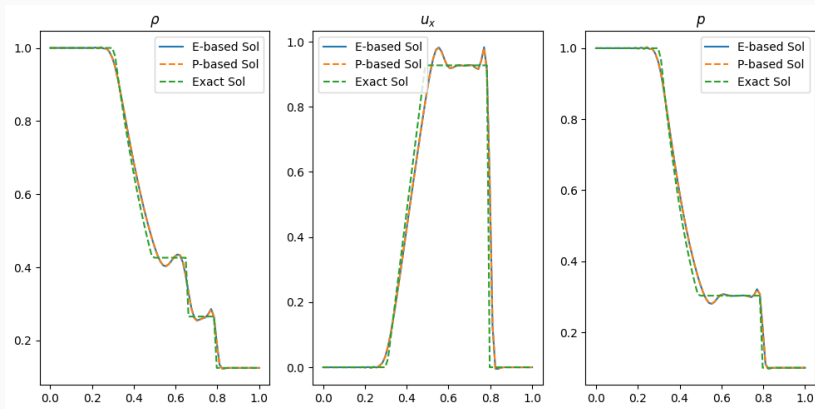


Figure 5: Numerical vs exact solution

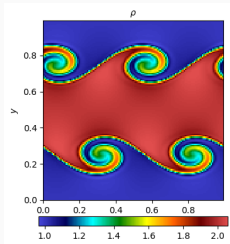
Kelvin–Helmholtz instability (setup)

Physics. Shear layer between fluids of different densities becomes unstable, rolling up into vortices and turbulence [4].

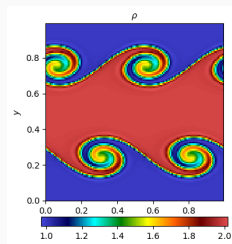
setup (no gravity)

- Domain $\Omega = [0, 1]^2$, periodic in x, y ; constant pressure $p_0 = 2.5$.
- Smooth layers of thickness $L = 0.025$: $(\rho_1, \rho_2) = (1, 2)$, $(u_1, u_2) = (+0.5, -0.5)$.
- Vertical seed perturbation: $u_y(x, y, 0) = \varepsilon \sin(4\pi x)$, $\varepsilon = 10^{-2}$.
- Grid 128×128 , final time $t = 2$; Mach numbers $M \in \{1, 10^{-1}, 10^{-2}, 10^{-3}\}$.

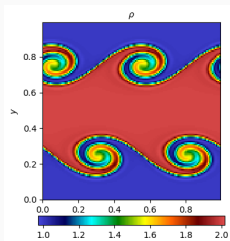
Note The *pressure-based* scheme yields qualitatively the same roll-up and vortex pairing.



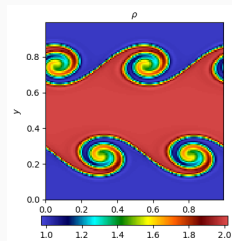
(a) $M = 1$



(b) $M = 10^{-1}$



(c) $M = 10^{-2}$



(d) $M = 10^{-3}$

Figure 6: Density at $t = 2$ (second-order scheme, Energy-based formulation).

Rayleigh–Taylor instability (setup)

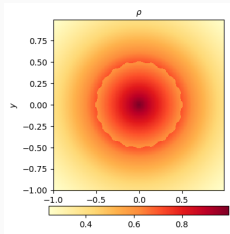
Goal. Assess the scheme's ability to capture gravity-driven interface instabilities while preserving hydrostatic balance [8, 3].

Configuration.

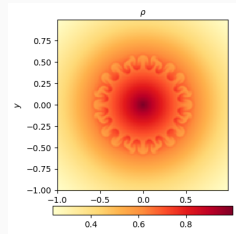
- Radial gravity with potential $\phi(r) = r$ (gravity points to the origin).
- Domain $D = [-1, 1] \times [-1, 1]$; grid 240×240 ; Mach $M = 1$.
- Base state: *isothermal hydrostatic equilibrium* with piecewise p, ρ ensuring pressure continuity via $\mu = \frac{e^{-r_0}}{e^{-r_0} + \Delta\rho}$.
- Perturbed interface $r_i(\theta) = r_0(1 + \nu \cos(k\theta))$.

Parameters. $r_0 = 0.5$, $\Delta\rho = 0.1$, $\nu = 0.02$, $k = 20$.

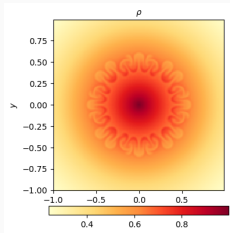
Note The pressure-based scheme exhibits the same qualitative behavior for this test case.



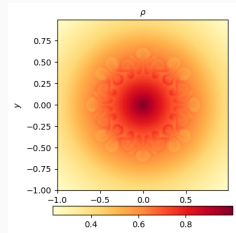
(a) $t = 0$



(b) $t = 2.9$



(c) $t = 3.8$



(d) $t = 5$

Figure 7: Rayleigh-Taylor instability in density (using Energy-based schema)

Rising bubble (setup)

Goal. Warm bubble rising in a stably stratified atmosphere [7].

Configuration.

- Domain $D = [0, 10] \times [0, 15]$ km; gravity in the y -direction with potential $\phi(x, y) = g y$, $g = 9.81 \text{ m s}^{-2}$.
- Base state: isentropic stratification expressed via the potential temperature $\theta = T \left(\frac{p_0}{p} \right)^{R/c_p}$, with $p_0 = 10^5 \text{ Pa}$, $R = c_p - c_v$, and $\gamma = 1.4$.
- Bubble perturbation in θ : $\delta\theta(x, y) = \theta_0 \cos^2\left(\frac{\pi r}{2}\right)$ for $r \leq 1$, otherwise 0, where $r = \sqrt{\left(\frac{x-x_c}{r_0}\right)^2 + \left(\frac{y-y_c}{r_0}\right)^2}$; center $(x_c, y_c) = (5, 2.75) \text{ km}$, radius $r_0 = 2 \text{ km}$, amplitude $\theta_0 = 6.6 \text{ K}$.
- Non-dimensionalization: reference scaling; in the tests we take $M = Fr = 10^{-2}$.

Note The pressure-based formulation displays the same qualitative evolution for the rising-bubble.

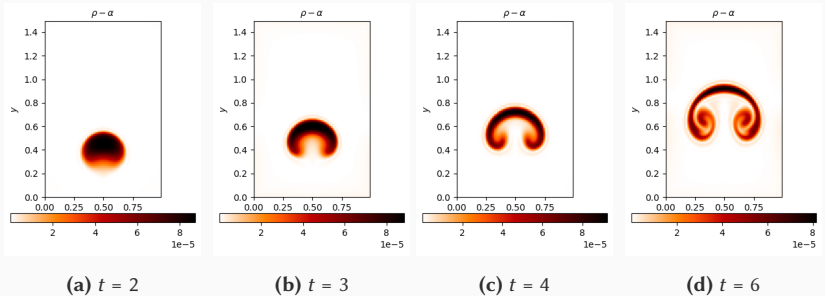


Figure 8: Density perturbation (using Energy-based schema)

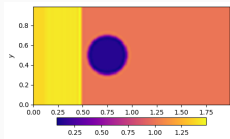
Shock–bubble interaction (setup)

Goal. Assess shock–bubble deformation and interface roll-up in a strong-shock setting [5].

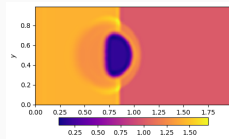
Configuration.

- 2D Euler (without gravity), ideal gas ($\gamma = 1.4$); domain $D = [0, 2] \times [0, 1]$.
- $u = v = 0, p = 1$.
- Density: $\rho = \rho_{\text{bubble}} = 0.138$ inside the circular bubble, $\rho_R = 1.0$ (right state), $\rho_L = 1.3764$ (left state).
- Incident planar shock of Mach $M_s = 1.22$ (propagating from the left).

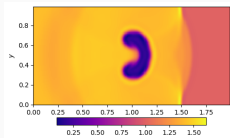
Note. The pressure-based formulation exhibits the same qualitative behavior.



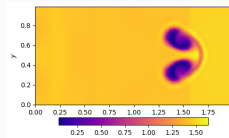
(a) $t = 0.2$



(b) $t = 0.5$



(c) $t = 1.0$



(d) $t = 2.0$

Figure 9: Shock–bubble interaction: density snapshots (using energy-based scheme)

Conclusion

Conclusion

Contributions.

- Developed semi-implicit, **well-balanced** schemes for the Euler equations with gravity.
- Designed for **low-Mach robustness** while **exactly preserving** hydrostatic equilibria (AP behavior).
- **Validation:** Across benchmarks (Kelvin–Helmholtz, Rayleigh–Taylor, rising bubble, shock–bubble).

Challenges.

- Ensuring stability at **very low Mach** numbers and in long-time integrations (avoid spurious oscillations).

Outlook.

- Increase accuracy to **fourth order**.
- Explore advanced applications in **geophysical** and **astrophysical** flows.

Thank you for your attention!

Questions?

Bibliography

Bibliography i



Sebastiano Boscarino, Giovanni Russo, and Leonardo Scandurra.
All mach number second order semi-implicit scheme for the euler equations of gas dynamics.

Journal of Scientific Computing, 77(2):850–884, 2018.



Leonhard Euler.
Principia motus fluidorum.

Novi Commentarii Academiae Scientiarum Petropolitanae, 6:271–311, 1761.



Randall J. LeVeque and Derek S. Bale.
Wave propagation methods for conservation laws with source terms.

In *Hyperbolic Problems: Theory, Numerics, Applications. Seventh International Conference in Zürich, February 1998, Volume II*, pages 609–618, Basel, 1999. Birkhäuser.

Bibliography ii



Colin P. McNally, Wladimir Lyra, and Jean-Claude Passy.
A well-posed kelvin–helmholtz instability test and comparison.
The Astrophysical Journal Supplement Series, 201(2):18, 2012.



James J. Quirk and Smadar Karni.
On the dynamics of a shock–bubble interaction.
Journal of Fluid Mechanics, 318:129–163, 1996.



Gary A. Sod.
A survey of several finite difference methods for systems of nonlinear hyperbolic conservation laws.
Journal of Computational Physics, 27(1):1–31, 1978.



Andrea Thomann, Gabriella Puppo, and Christian Klingenberg.
An all-speed second order well-balanced imex relaxation scheme for the euler equations with gravity.
Journal of Computational Physics, 420:109723, 2020.



Andrea Thomann, Markus Zenk, and Christian Klingenberg.

A second-order positivity-preserving well-balanced finite volume scheme for euler equations with gravity for arbitrary hydrostatic equilibria.

International Journal for Numerical Methods in Fluids, 89(11):465–482, 2019.